Core transport analysis of nitrogen seeded H-mode discharges in the ASDEX Upgrade

2013 Plasma Phys. Control. Fusion 55 015010

(http://iopscience.iop.org/0741-3335/55/1/015010)

Plasma Phys. Control. Fusion **55** (2013) 015010 (6pp) doi:10.1088/0741-3335/55/1/015010

Core transport analysis of nitrogen seeded H-mode discharges in the ASDEX Upgrade

G Tardini, R Fischer, F Jenko, A Kallenbach, R M McDermott, T Pütterich, S K Rathgeber, M Schneller, J Schweinzer, A C C Sips, D Told, E Wolfrum and the ASDEX Upgrade Team

Max-Planck-Institut für Plasmaphysik, EURATOM Association, Boltzmannstraße 2, 85748 Garching, Germany

E-mail: git@ipp.mpg.de

Received 13 March 2012, in final form 9 November 2012
Published 7 December 2012
Online at stacks.iop.org/PPCF/55/015010

Abstract
In the all-tungsten ASDEX Upgrade tokamak nitrogen seeding is a reliable method for radiative cooling at the plasma edge, regularly applied in high power scenarios. Interestingly, in the presence of nitrogen seeding the energy confinement is observed to improve significantly, compared with similar unseeded discharges, with an increase by 10–25% in plasma stored energy and $H_{\mathrm{IPB98}(y,2)}$. In this paper, we document the improvement and we analyse the transport properties in the core plasma, by comparing similar discharges with and without nitrogen seeding. The increase in the suprathermal energy content is assessed as well. The impurity nitrogen is shown not to penetrate significantly into the core plasma. Non-linear gyro-kinetic simulations predict that the improvement observed in the pedestal confinement is transferred to the core via profile stiffness, in agreement with the experimental evidence, whereas the direct contribution from core confinement is small.

(Some figures may appear in colour only in the online journal)

1. Introduction

The control of the heat flux through the divertor is expected to be crucial in tokamaks with a burning plasma such as ITER.

In the ASDEX Upgrade tokamak a tungsten wall has been implemented stepwise over several years, to study alternative first wall materials other than carbon for a future tokamak reactor [1]. The coating of all carbon tiles was completed in 2006. The consequent decrease in the radiated power in the edge and divertor regions has stimulated recipes to control the heat load on the divertor plates at high heat flux as required, for instance, by hybrid scenarios such as the improved H-mode in ASDEX Upgrade [2]. Tungsten is not affordable as a radiative cooler, since any significant inflow from the first wall often leads to tungsten accumulation in the core and to a radiative collapse, in particular under conditions with good confinement. In order to control the power load to the divertor, a typical technique is to apply low to medium Z impurity seeding, especially nitrogen or argon; this has been investigated experimentally in several tokamaks like TEXTOR-94 [3] and in almost all divertor devices like JET [4], JT-60 [5], DIII-D [6] and also in tokamaks with high-Z facing components such as ASDEX Upgrade [7] and Alcator C-Mod [8]. In ASDEX Upgrade nitrogen puff is applied as the routine actuator for the real time control of the divertor temperature, while a possible accumulation in the core is prevented by applying central electron cyclotron resonance heating (ECRH) [9]. Despite the higher radiated power, the plasma stored energy is higher in a nitrogen seeded discharge than in a similar one without seeding, with a significant increase in $H_{\mathrm{IPB98}(y,2)}$ by 10–25% [9, 10]. In section 2, we document the confinement improvement, which turns out to be very reproducible and robust over a variety of plasma parameters and heating schemes. The core profile characteristics with and without nitrogen seeding are presented in section 3, including a discussion of the inferred impurity density profiles. In section 4, the core heat transport is predicted by means of non-linear gyrokinetic simulations,

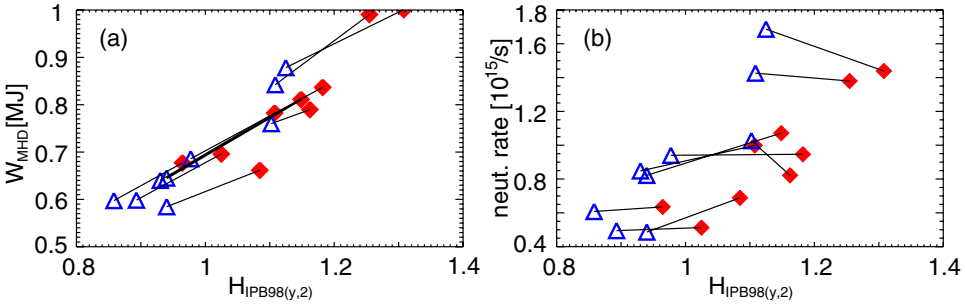

Figure 1. (*a*) Plasma stored energy versus $H_{\mathrm{IPB98}(y,2)}$; (*b*) neutron rate as a function of $H_{\mathrm{IPB98}(y,2)}$. For unseeded (empty blue triangles) and seeded (full red squares) discharges. Lines connect discharge pairs. N_2 seeding enhances the stored plasma energy and $H_{\mathrm{IPB98}(y,2)}$, whereas the neutron rate does not increase significantly.

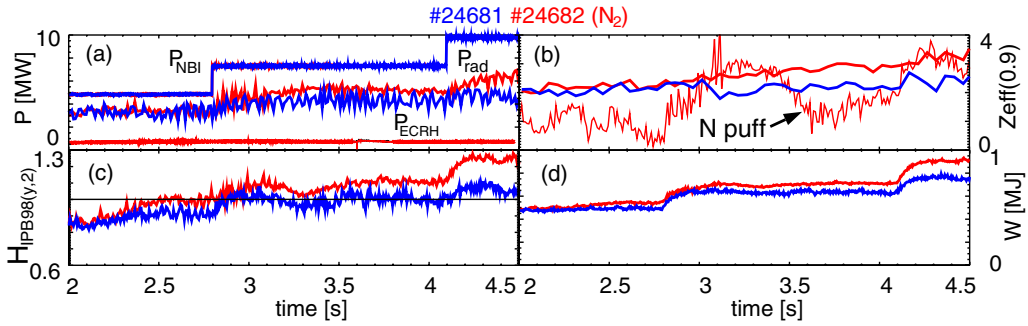

Figure 2. Time traces of the heating power (*a*), Z_{eff} at $\rho_{\mathrm{tor}} = 0.9$ (*b*), $H_{\mathrm{IPB98}(y,2)}$ (*c*), plasma stored energy (*d*). Discharge #24682 (red) is seeded, #24681 (blue) is unseeded.

confirming that the core contribution to the confinement improvement is small. Finally, conclusions are drawn in section 5.

2. Nitrogen seeding and global confinement

The beneficial effect of seeding on the overall confinement has been observed in the tungsten coated ASDEX Upgrade [9, 10]. A database comparison between seeded and unseeded discharges is shown in figure 7(*a*) in [11]. The confinement improvement factor $H_{\mathrm{IPB98}(y,2)}$ is systematically higher for seeded discharges by 10–25% [9]. It is even better than the confinement observed in the older improved H-mode discharges (figure 7(*a*) in [11]) from the carbon dominated ASDEX Upgrade. However, the overlap of the collisionality ranges is rather small due to the difficulty to access low density with the tungsten-coated wall.

Since the confinement improvement appears robust and clearly beyond the data scattering, dedicated pairs of similar discharges have been performed in order to allow a direct comparison under identical engineering parameters and similar plasma parameters. Moreover, a direct comparison of the energy content and of the kinetic profiles should exclude the possibility that the higher $H_{\mathrm{IPB98}(y,2)}$ might be an artefact of the underlying scaling law [12] or of an experimental setup, such as different power mix. In the discharge pairs the electron density was not feedback-controlled, but it was kept constant with a high gas puff rate and by applying central ECRH, which is known to robustly prevent impurity accumulation in ASDEX Upgrade H-mode plasmas [13]. Discharge pairs were performed in most cases in successive discharges, in order to reproduce the machine conditioning. The discharge pairs confirmed the observed trend of higher confinement in the presence of N_2 seeding, as illustrated in figure 1. The lines in figure 1 connect pairs of similar discharges. The confinement factor $H_{\mathrm{IPB98}(y,2)}$ always improves with N_2 seeding, by a variable amount ranging between 10% and 25%. The same happens for the plasma stored energy (figure 1(*a*)), confirming that the improvement in $H_{\mathrm{IPB98}(y,2)}$ is no artifact of the scaling laws. Interestingly, the neutron rate does not increase significantly in the seeded discharge, or not at all, despite the higher confinement (figure 1(*b*)). This suggests that the impurity content might be indeed different, diluting the deuterium fuel for D–D reactions, in particular for beam-target reactions, which are found to be dominant in ASDEX Upgrade H-mode plasmas [14]. This decrease compensates partly the increase in the beam-target neutron production associated with the higher suprathermal population, which is a consequence of the higher T_e and hence higher slowing-down time. This will be discussed in detail in section 3.2.

Typical time traces of the seeded and unseeded discharges are compared in figure 2. In particular, the power steps are performed at the same time and both the NBI and ECRH power levels are matched. N_2 seeding is applied in discharge #24682 as a feedback actuator on the divertor temperature, causing the strong time variation seen in figure 2(*b*). Moreover, at every power step there is an increase in the N_2 puffing rate, as a result of the feedback on the divertor temperature.

The energy content is higher in the seeded discharge. This is a general observation, despite the higher radiated power (see figure 2). In general, for improved H-modes a favourable scaling of $H_{\mathrm{IPB98}(y,2)}$ with auxiliary power has been

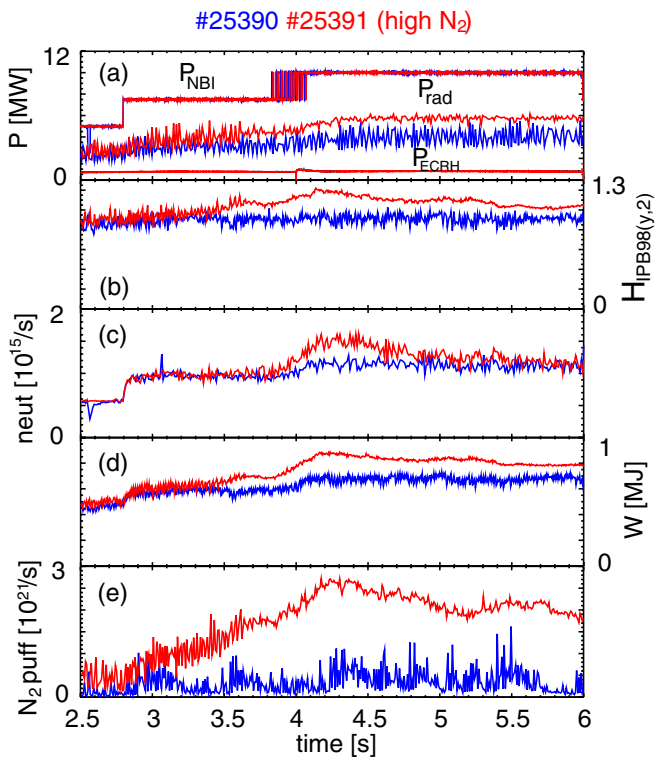

Figure 3. Time traces of discharge #25390 (blue), with negligible N_2 seeding, and the seeded discharge #25391 (red).

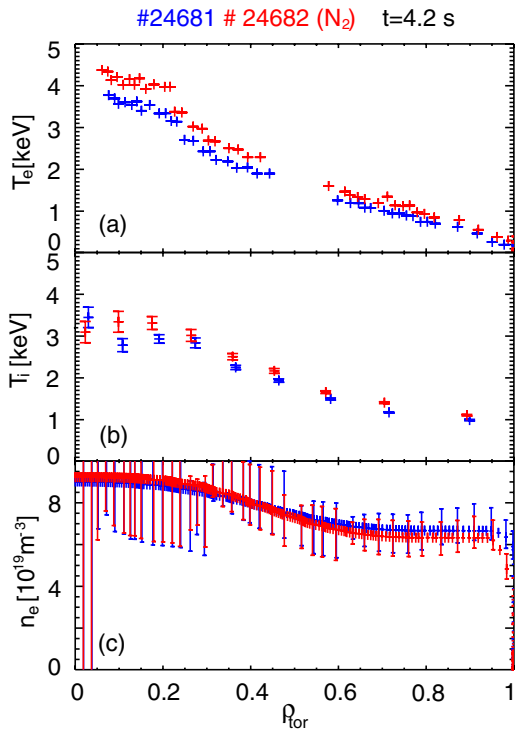

Figure 4. Kinetic profiles of the unseeded discharge #24681 (blue) and the seeded one #24682 (red). (*a*) Electron temperature from electron cyclotron emission (*b*) ion temperature from charge exchange recombination and (*c*) electron density from integrated data analysis.

observed [15]. On top of this, the confinement improvement $\Delta H_{\mathrm{IPB98}(y,2)}$, i.e. the difference in $H_{\mathrm{IPB98}(y,2)}$ between the seeded and the unseeded discharge, is more pronounced at high power, so that overall there is a superposition of both confinement improvements. This power dependence is likely due to the higher nitrogen puff rate applied in the presence of strong auxiliary heating, in order to keep the divertor temperature sufficiently low.

As expected, Z_{eff} at $\rho_{\mathrm{tor}} = 0.9$ (figure 2(*b*)) is higher for the seeded discharge, with the difference becoming more significant in time, i.e. either with increasing power or, more likely, with increasing N_2 content due to the continuous puffing. The pair displayed in figure 2 was obtained a long time after the last boronization, just to demonstrate the robustness of the improvement even in the absence of the optimal machine conditioning. Discharge pairs performed shortly after a boronization exhibited a very similar behaviour. An example of this is shown in figure 3. Here the density was around 6×10^{19} m^{-3}, lower than for the pair #24681 #24682, where it was roughly 8×10^{19} m^{-3}. Again, the confinement factor benefits from the N_2 seeding, increasing up to 25% in the most favourable phase around 4.4 s. Interestingly, #25390 also happens to have a weak N_2 puff, showing that the effect is not just qualitative, but it depends on the amount of N_2 injected.

3. Core profile characteristics of nitrogen seeded discharges

Discharge pairs allow a direct comparison of the profile properties. In particular, the kinetic profiles show which channel features improved transport properties, and in which plasma region. Despite the significant variations in plasma density, auxiliary heating and machine conditioning within our database, the kinetic profiles of discharge pairs exhibit similar behaviours, illustrated in figure 4 for one pair. The density profile is almost unchanged by adding N_2 seeding. This is beneficial for the transport analysis, since different density profiles would lead to different beam penetration and hence different heat flux profiles. Typically, in ASDEX Upgrade H-mode plasmas the main instability is either the trapped electron mode (TEM) or the ion temperature gradient (ITG) driven mode [16]. If the density peaking were significantly different between the seeded and the unseeded discharge then the dominant instability could change. As a consequence, the transport properties of the plasma would be significantly modified [17]. In fact, seeded discharges occasionally exhibit stronger peaking of the electron density profile. However, even in those cases the increase in the density peaking is small, as shown in figure 4(*c*). It is a general observation for discharge pairs that both ion and electron temperature profiles are higher in the core for seeded discharges. This is true also at the pedestal top, but the core temperature gradients are higher as well. The ion and electron temperature profiles are presented in figures 4(*a*) and (*b*). The seeded case has larger temperature gradients in the core region, but the gradient lengths $L_T = |\nabla T|/T$ are the same [18]. In other words, the core confinement improvement is a consequence of the higher pedestal temperature, which is then propagated towards the plasma centre via profile stiffness [16].

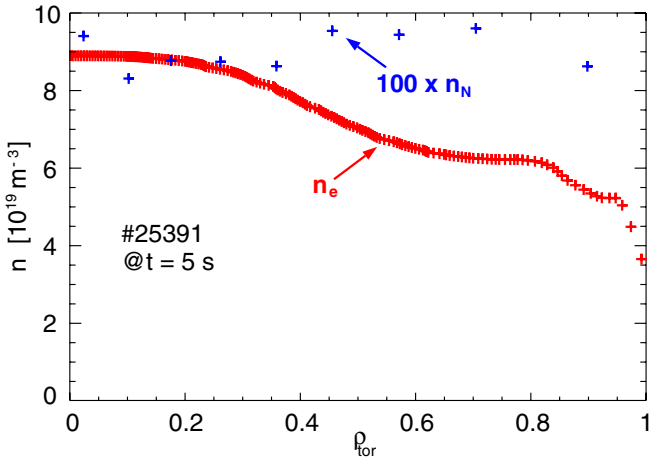

Figure 5. $100 \times n_N$ (blue) from charge exchange spectroscopy for the discharges for discharge #25391 with N_2 seeding, superimposed to the n_e profile (red).

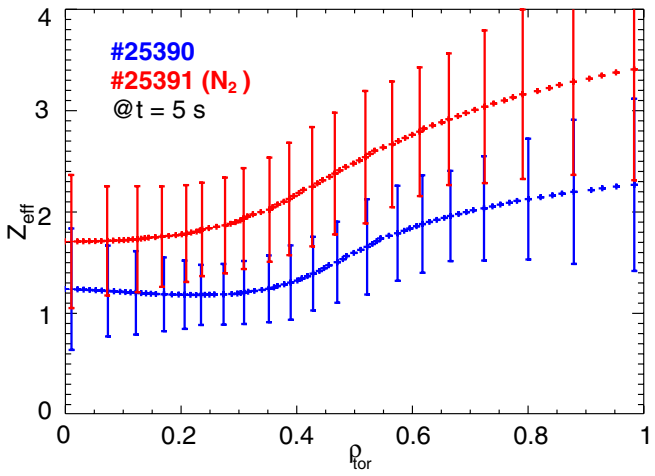

Figure 6. Effective charge profile from bremsstrahlung for the discharges #25390 (blue), without N_2 seeding, and #25391 (red), with.

It has to be noted that in the all-tungsten ASDEX Upgrade low plasma densities are not accessible. Due to the high plasma density, the electron and ion temperatures are close to each other due to the rapid heat exchange between species. So it is not obvious, *a priori*, which channel is responsible for the confinement improvement. Detailed turbulent stability and transport calculations are required and will be presented in section 4.

3.1. The impurity density profile

The charge exchange recombination of the nitrogen line at $\lambda = 566.9$ nm delivers a direct measurement of the nitrogen density profile n_N, shown in figure 5. The nitrogen concentration $c_N = n_N/n_e$ appears to be 1% for $\rho_{tor} \leqslant 0.4$ and roughly 1.5% outside. This is perfectly consistent with the independent measurement of the effective charge (Z_{eff}) profile via bremsstrahlung [19] (see figure 6). In fact, the other main impurities contributing to Z_{eff} are carbon and boron (in the case of recent boronization, as it is the case for #25391) [20],

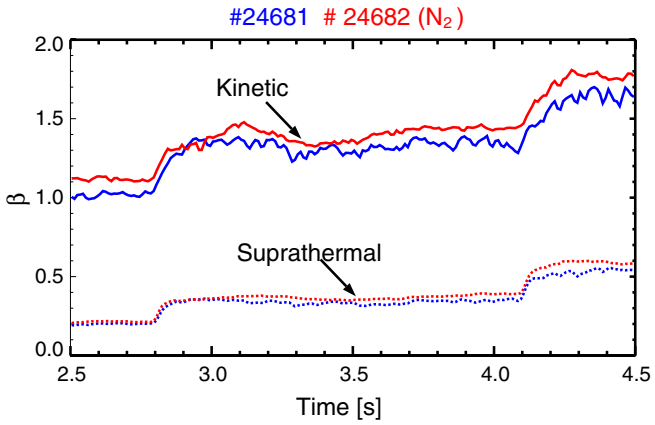

Figure 7. Kinetic and suprathermal β for the unseeded discharge #24681 (blue) and the seeded one #24682 (red). The thermal contribution dominates the confinement improvement.

both with similar Z as nitrogen. Since $Z_N = 7$, a nitrogen concentration of $c_N = 1\%$ corresponds to a $\Delta Z_{eff} = 0.42$, assuming nitrogen to be the only impurity. According to figure 6, the strongest Z_{eff} variation in the N_2 seeded case occurs at the plasma edge. This is the optimum situation, since it enables the radiative cooling of the plasma near the divertor, without having a strong impurity penetration in the plasma core, which could lead to accumulation. The measured 2D emissivity profile from the bolometry confirms the localisation of the radiation near the separatrix and in particular near the divertor, as shown in figure 1(*b*) in [21].

3.2. The impact of the fast ion energy

The electron temperature is higher by 10% up to 20% in the seeded case. As a consequence, the NBI fast ions slowing-down time is also longer and, therefore, the fast ion pressure is larger. In the seeded discharge # 24682 at 4.2 s the slowing time is higher than for # 24681 by 15%, the fast ion pressure by 10%. This effect can occur only on top of a pre-existing thermal improvement, i.e. if the electron temperature is higher (or if the plasma density is lower, but this is not observed). Nevertheless, it accounts for a fraction of the higher energy content in seeded discharges.

The impact of the change in fast ion pressure on the total β has been studied by simulating the NBI with the TRANSP-NUBEAM code [22] (see figure 7). The suprathermal energy content ranges for both discharges between 20% and 30% of the kinetic energy, and increases for higher NBI power, which has steps at 2.8 and 4.1 s . In the nitrogen seeded shot # 24682 both the suprathermal and the kinetic contribution increase, the latter providing the higher absolute variation. Nevertheless, the fast ion β plays a non-negligible role, increasing by an amount of 1–5% of the total β, depending on the NBI power, whereas the improvement due to the thermal contribution is around 10%.

According to the TRANSP simulations, 85% of the neutrons are generated by beam–target reactions in these discharges. The higher fast ion content shown in figure 7 should, therefore, correspond to a higher neutron production

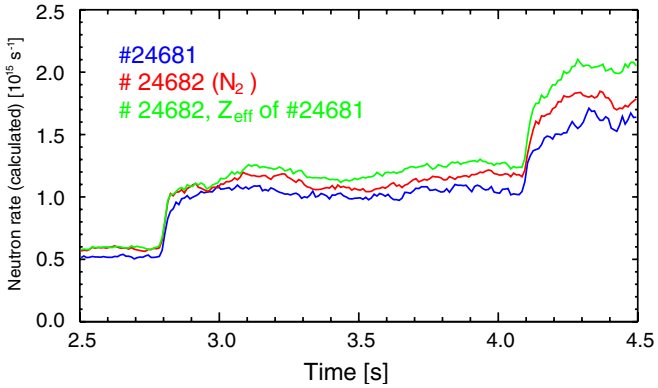

Figure 8. TRANSP calculation of the neutron rate for the unseeded discharge #24681 (blue) and the seeded one #24682 with the measured $Z_{\rm eff}$ profile (red) and with the $Z_{\rm eff}$ profile from discharge #24681 (green).

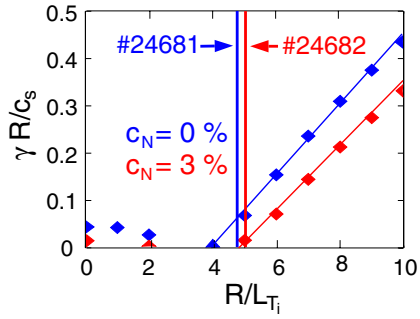

Figure 9. Growth rate of the ITG instability as calculated with the gyrokinetic code GS2 versus $R/L_{T_{\rm i}}$ at $\rho_{\rm tor} = 0.5$, assuming $c_{\rm N} = 0$ (blue) and $c_{\rm N} = 3\%$ (red). The simulations assume $k\rho_{\rm i} = 0.3$. The vertical lines correspond to the respective experimental values of $R/L_{T_{\rm i}}$ in discharges #24681 and #24682.

rate. However, the higher $Z_{\rm eff}$ in the seeded discharge acts in the opposite direction. To quantify these competing effects, we have performed a third simulation on top of those presented in figure 7. There the seeded discharge #24682 is simulated assuming the $Z_{\rm eff}$ profile from the unseeded #24681 in order to decouple the effects of the different fast ion population and $Z_{\rm eff}$ profile. The result are shown in figure 8, where the "artificial" simulation is the green curve. The higher fast ion content is responsible for a 10–20% increase in the neutron rate, as the comparison between the blue and the green curve highlights. The higher $Z_{\rm eff}$ limits this increase to roughly one half (red curve) compared with the improvement exhibited in the green time trace, i.e. only 5–10% higher than the unseeded case (blue). The competition between higher fast ion content and $Z_{\rm eff}$ in the seeded discharge is consistent with the trend shown in figure 1, where the neutron rate increases less than $H_{\rm IPB98(y,2)}$, or not at all.

4. Gyrokinetic prediction of core transport

The experimental uncertainties for $n_{\rm e}$, $\nabla T_{\rm i}$ and $\nabla T_{\rm e}$ are too large for a power balance analysis to resolve a possible difference in the effective heat diffusivities between discharges with and without N_2 seeding. However, the TRANSP code [22] is used to calculate the ion and electron heat fluxes and to provide a reference heat flux for the gyrokinetic simulations.

A linear stability analysis with the code GS2 [23] is performed as a function of $R/L_{T_{\rm i}}$. The background parameters such as $T_{\rm e}$, $T_{\rm i}$, $n_{\rm e}$, $\nabla n_{\rm e}$, $\nabla T_{\rm e}$, $\hat{s}$ and q are taken from the experimental measurements of the unseeded discharge # 24681. In the first $R/L_{T_{\rm i}}$ scan (blue curve in figure 9) a pure deuterium plasma is assumed, while in the second scan a nitrogen impurity is added to see its direct effect on the instability threshold. The nitrogen concentration is chosen to be 3%, which is the upper limit of the measured profiles including possible uncertainties. The simulation results are shown in figure 9 for $k_\theta \rho_{\rm i} = 0.3$, where k_θ is the perpendicular wave number and $\rho_{\rm i}$ the ion Larmor radius. Both electron–ion and electron–electron collisions are included in the simulations. The dominant mode at half radius turns out to be the ITG, whenever $R/L_{T_{\rm i}} > 4$–5. This is expected due to the medium-high local collisionality value at $\rho_{\rm tor} = 0.5$: in the pure deuterium case it is $\nu_{\rm ei} R/c_{\rm s} = 0.37$, in the seeded case $\nu_{\rm ei} R/c_{\rm s} = 0.81$. There $\nu_{\rm ei} = 0.089 R Z_{\rm eff} n_{\rm e}/T_{\rm e}^2$ is the electron-ion collision frequency and $c_{\rm s} = \sqrt{T_{\rm e}/m_D}$ the deuterium sound velocity. As reported in [24], the ITG mode dominates in almost all cases for $\nu_{\rm ei} R/c_{\rm s} > 0.3$ and the typical experimental value $R/L_{T_{\rm i}} \approx 5$. The mode appears to be mitigated in the presence of nitrogen seeding, due to the deuterium dilution associated with a higher impurity content, so that the critical ITG threshold in figure 9 is upshifted in the seeded case. This dilution effect is a known stabilizing mechanism for the ITG, it has already been invoked to explain the radiative improved regime in TEXTOR [25] and for ion heat transport barriers in ASDEX Upgrade [26]. However, only non-linear calculations at a given heat flux can assess the quantitative impact of N_2 seeding on the temperature gradients. The gyrokinetic code GENE [27] is used for a scan of $\nabla T_{\rm i}$, taking the experimental values for the input parameters $T_{\rm e}$, $T_{\rm i}$, $n_{\rm e}$, $\nabla n_{\rm e}$, $\nabla T_{\rm e}$, $\hat{s}$ and q for each discharge, in particular the local temperature values, which are higher by 15–20% in the seeded discharge. It is found that the predicted modification of $R/L_{T_{\rm i}}$ and $R/L_{T_{\rm e}}$ at the relevant heat flux level is negligible in the case considered, as illustrated in figure 10. At half radius (figure 10(*a*)) the critical threshold shows no upshift, in contrast to the linear result. At $\rho_{\rm tor} = 0.8$ the critical threshold for $R/L_{T_{\rm i}}$ is higher for the seeded discharge, but the stronger profile stiffness associated with a higher $T_{\rm e}$ compensates this shift, since the ITG driven heat flux above criticality scales like $T_{\rm e}^{\frac{5}{2}}$. As a consequence, at the relevant heat fluxes $R/L_{T_{\rm i}}$ is the same. This is consistent with the experimental result shown in [9]. The confinement improvement is therefore mainly occurring at the plasma edge, the profile stiffness simply extends the improvement to the core region by constraining the temperature profiles to a fixed $R/L_{T_{\rm i}}$.

5. Conclusions

The confinement improvement in N_2 seeded discharges is a robust observation, as it occurs at different heating power levels, with and without boronization and for different plasma

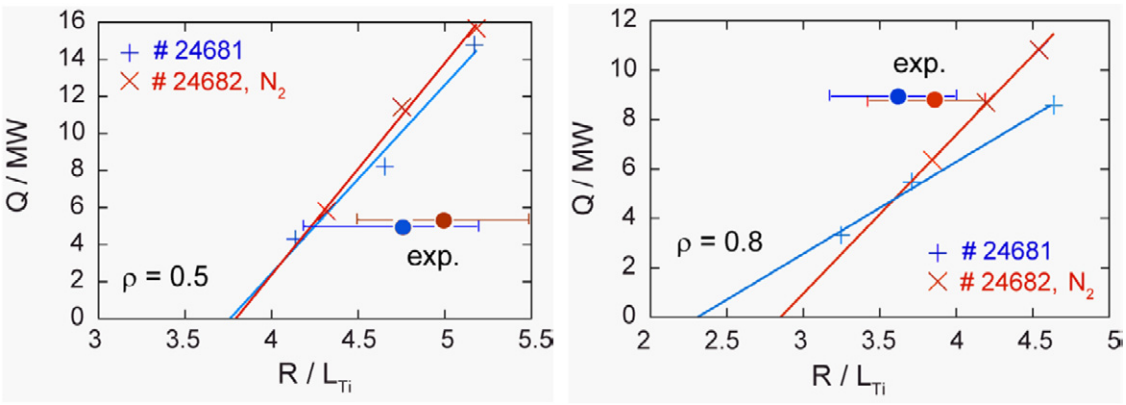

Figure 10. R/L_{T_i} scan with the non-linear gyrokinetic code GENE, at $\rho_{tor} = 0.5$ (*a*) and at $\rho_{tor} = 0.8$ (*b*). The full circles represent the heat flux simulated with TRANSP and the measured R/L_{T_i}.

densities. On top of the general improvement of $H_{IPB98(y,2)}$ with increasing auxiliary power for improved H-modes, also the Δ $H_{IPB98(y,2)}$ due to nitrogen seeding shows a positive dependence on the heating power, which is correlated with a higher N_2 puff rate in order to keep the divertor temperature sufficiently low. The improved edge diagnostic coverage in ASDEX Upgrade allows the kinetic profiles in the pedestal region to be resolved; the measurements show that the confinement improvement in N_2 seeded discharges is largely an edge effect, as the pedestal pressure increases by up to 20%. In the core, despite the overall increase of T_e and T_i, no significant enhancement in R/L_{T_i} is observed in general. Gyrokinetic non-linear simulations predict a negligible shift in the critical gradient length in the presence of nitrogen at half radius, whereas at the pedestal top an upshift is observed. However, there the increase in the critical R/L_{T_i} is compensated by higher profile stiffness due to higher T_e, yielding only a negligible change in the core gradient length, consistent with the experimental observations within the measurement uncertainties. The density peaking can slightly increase in the presence of N_2 seeding, but in most cases it remains unchanged. Its effect on the energy confinement at medium-high density is negligible. The suprathermal contribution to the stored plasma energy is higher in the seeded case because the higher T_e enhances the NBI fast ions slowing-down time. This can account for a fraction of the total confinement improvement, but it is not the dominant term.

References

[1] Neu R *et al* 2007 *Plasma Phys. Control. Fusion* **49** B59
[2] Gruber O *et al* 2009 *Nucl. Fusion* **49** 115014
[3] Messiaen A M *et al* 1994 *Nucl. Fusion* **34** 825
[4] Maddison G P *et al* 2003 *Nucl. Fusion* **43** 49
[5] Kubo H *et al* 2001 *Nucl. Fusion* **41** 227
[6] Jackson G L *et al* 2002 *Nucl. Fusion* **42** 28
[7] Kallenbach A *et al* 2010 *Plasma Phys. Control. Fusion* **52** 055002
[8] Hughes J W *et al* 2001 *Nucl. Fusion* **51** 083007
[9] Schweinzer J *et al* 2011 *Nucl. Fusion* **51** 113003
[10] Tardini G *et al* 2009 *Proc. 36th EPS Conf. on Plasma Physics (Sofia, Bulgaria)* vol 33E O-2.004
[11] Kallenbach A *et al* 2011 *Nucl. Fusion* **51** 094012
[12] ITER Physics Expert Group on Confinement and Transport, ITER Physics Expert Group on Confinement Modelling and Database and ITER Physics Basis Editors 1999 *Nucl. Fusion* **39** 2175
[13] Angioni C *et al* 2007 *Phys. Plasmas* **14** 055905
[14] Höhbauer C 2010 Modellierung der Neutronenproduktion in Plasmaentladungen am Fusionsexperiment ASDEX Upgrade *IPP Report* 1/339
[15] Maggi C F *et al* 2007 *Nucl. Fusion* **47** 535
[16] Tardini G *et al* 2002 *Nucl. Fusion* **42** 258
[17] Angioni C *et al* 2003 *Phys. Rev. Lett.* **90** 205003
[18] Tardini G *et al* 2010 *Proc. 37th EPS Conf. on Plasma Physics* (Dublin, Ireland) P1.1097
[19] Rathgeber S *et al* 2010 *Nucl. Fusion* **50** 035012
[20] Kallenbach A *et al* 2009 *Nucl. Fusion* **49** 045007
[21] Fuchs J C *et al* 2011 *J. Nucl. Mater.* **415** S852
[22] Pankin A, McCune D and Andre R *et al* 2004 *Comput. Phys. Commun.* **159** 157
[23] Kotschenreuther M *et al* 1995 *Phys. Plasmas* **2** 2381
[24] Angioni C *et al* 2005 *Phys. Plasmas* **12** 040701
[25] Tokar M Z *et al* 1999 *Plasma Phys. Control. Fusion* **41** L9
[26] Tardini G *et al* 2007 *Nucl. Fusion* **47** 280
[27] Jenko F *et al* 2000 *Phys. Plasmas* **7** 1904